We are IntechOpen,
the world's leading publisher of
Open Access books
Built by scientists, for scientists

6,900
Open access books available

186,000
International authors and editors

200M
Downloads

Our authors are among the

154
Countries delivered to

TOP 1%
most cited scientists

12.2%
Contributors from top 500 universities

CLARIVATE ANALYTICS
BOOK CITATION INDEX
INDEXED

WEB OF SCIENCE™

Selection of our books indexed in the Book Citation Index
in Web of Science™ Core Collection (BKCI)

Interested in publishing with us?
Contact book.department@intechopen.com

Optical, Excitonic, and Electronic Properties of CH₃NH₃PbI₃ Thin Films and Their Application in Photovoltaics

Sheng Hsiung Chang, Hsin-Ming Cheng, Sheng-Hui Chen and Kuen-Feng Lin

Additional information is available at the end of the chapter

Abstract

In the past two years, the highest power conversion efficiency of perovskite absorber (PA)–based photovoltaics has been 20.2%. The PA can be fabricated on flat substrates (for example, ZnO, TiO₂, and PEDOT:PSS) using solution processes, which have a low-cost advantage in terms of industry production. In this report, the recent advances of PA-based photovoltaics will be mentioned. Then, the optoelectronic properties of PA, material fabrication, and photovoltaic performance will be discussed. On the other hand, we used scanning electron microscopy, two-dimensional X-ray diffractometer, and photoluminescence spectroscopy to investigate the fundamental properties of CH₃NH₃PbI₃ thin films fabricated with and without toluene washing treatment, which provides an assessment of the development potential of PA-based photovoltaics.

Keywords: Perovskite photovoltaic, Exciton, Nanoplasmonic structure, 2D X-ray diffraction

1. Introduction

The perovskite structure is named after the structure of calcium carbonate ($CaTiO_3$) compound and its molecular formula is ABX_3. Perovskite oxide materials ($SrTiO_3$ and $LaAlO_3$) [1] and nonoxide perovskite materials ($MgCNi_3$) [2] have high-temperature superconductivity properties, which indicate that perovskite structures have excellent electrical properties. In the past two years, the most popular light-absorbing materials for photovoltaic cells have been organic–inorganic lead halide perovskite absorbers ($CH_3NH_3PbI_3$), in which absorption bandgap is approximately 1.57 eV [3] and exciton binding energy is less than 50 meV [4], hence

they have excellent power conversion efficiency (PCE). The molecular structure of the earliest application of perovskite materials in an optoelectronic device (($C_6H_5C_2H_4NH_3)_2PbI_4$) was in 1994, in Kyushu University, Japan, where Tsutsui's research focused on the fluorescence characteristics of materials via electrical excitation [5]. Additionally, the emission wavelength of the luminous element was 520 nm at a low temperature, the full-width at half-maximum (FWHM) of fluorescence was about 10 nm, and the luminance of the perovskite-based device was 10,000 cd/m^2 with an injection current density of 2 A/cm^2. The brightness of perovskite-based light-emitting diodes was equivalent to four to five times of the organic light-emitting diode. In April 2009, Miyasaka's research team from the University of Tokyo published the world's first article relating to perovskite-sensitized solar cells. Their study showed that $CH_3NH_3PbI_3$ and $CH_3NNH_3PbBr_3$ could convert sunlight into electrical energy as light-absorbing materials through dye-sensitized solar cell structures, and the obtained PCE was 3.81% [6]. Although the study was published in an important academic journal, it did not receive much attention because of poor efficiency. In 2012, Gratzel from the Swiss Federal Institute of Technology, Lausanne (EPFL), optimized the device parameters of the dye-sensitized solar cells to enhance the PCE to 7.28% [7] under 0.1 sunlight intensity. In the same year, Snaith led his research team from the University of Oxford in England to publish their research on organic–inorganic lead halide perovskite photovoltaics using solution process in a scientific journal. They used an insulator Al_2O_3 nanoparticle film to replace the TiO_2 nanoparticle film for the first time, and named the structure meso-superstructured solar cell (MSSC). Additionally, the PCE reached a record of 10.9% [8]. Since then, scientists have launched a series of battles for higher PCE. In July 2013, Bruschka and Pellet adopted a two-step solution process method to produce $CH_3NH_3PbI_3$ on the porous TiO_2 substrate and the efficiency obtained was 12.9% [9]. Also, in September 2013, Snaith produced high-quality perovskite light-absorbing materials using a vapor deposition method and obtained a PCE of 5.4% [10]. In addition, in July 2014, Professor Wu from the National Central University used $PC_{71}BM$ thin film as an electron transport layer and improved the PCE up to 16.3% [11]. In August 2014, Yang's team optimized the energy level of each layer of the solar cells and increased the PCE to 19.3% [12]. Gratzel and Park also optimized the proportion of CH_3NH_3I and PbI_2 in the two-step solution process method and achieved an average PCE of up to 16.3% (±0.35%) [13].

This chapter will describe the optoelectronic properties, molecular structure, and fabrication method of perovskite materials, and calculate the effects of the nanoplasmonic structure on exciton generation and the dissociation of perovskite materials. In addition, it will use scanning electron microscope (SEM), two-dimensional X-ray diffractometer (2D-XRD), UV-vis spectrometer and photoluminescence to explore the morphology, structure, and electronic and excitonic properties of $CH_3NH_3PbI_3$ thin films formed by a solution process with and without a nonpolar solvent washing treatment [14], and will discuss the development direction and potential of the perovskite photovoltaics.

2. The optical and electronic properties of perovskite absorbers

The perovskite structure is shown in Figure 1. According to the first-principles calculation, each CH_3NH_3 and Pb provides one and two electrons to I_3, and the structure of CH_3NH_3 and

Pb-I can maintain electric neutrality due to van der Waals force, so CH_3NH_3 cations hardly affect the characteristics of Pb in the conduction band and "I" determines the properties of the valence band [15]. Although the CH_3NH_3 cation has no significant effect on the electronic structure, the orientation of the CH_3NH_3 cation can influence the dielectric constant of $CH_3NH_3PbI_3$ materials. As shown in Table 1, the exciton binding energy can be calculated by $E_b = e^2 /[4\pi\varepsilon_0\varepsilon_d r]$, where, r is the Bohr radius (2.8 nm) [16] and ε_d is the dielectric constant [17] of $CH_3NH_3PbI_3$. Exciton binding energy is as low as possible to be more favorable for exciton self-dissociation at room temperature and exciton dissociation at the interface to produce photocurrent, so the orientation of CH_3NH_3 cation is very essential to excitonic properties. The most direct physical parameter for device efficiency is the exciton diffusion length. Snaith estimated that the exciton diffusion length could be over 1 μm, through measurement of the exciton's lifetime. The long diffusion length in poly-crystalline $CH_3NH_3PbI_3$ thin films has been directly observed using a spatial and temporal imaging system [18]. Therefore, photons can be effectively converted into photocurrent after being absorbed. Experimental results showed that the exciton lifetime of the perovskite materials could exceed 100 ns [19].
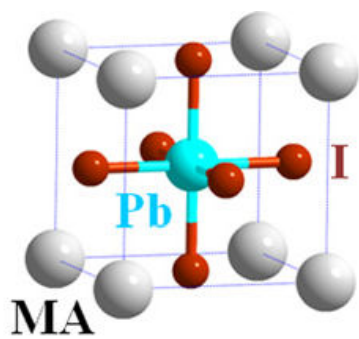

Figure 1. Perovskite structure. MA is [CH₃NH₃]⁺ [15].

CH₃NH₃ Orientation	ε_d (x, y, z)	E_b (x, y, z) (meV)
(001)	22.39, 27.65, 17.97	36.7, 29.7, 45.7
(011)	17.95, 23.56, 22.67	45.8, 34.9, 36.2
(111)	36.52, 37,28, 24.94	22.5, 22.0, 32.9

Table 1. Anisotropic dielectric constants and exciton binding energies of CH₃NH₃PbI₃ crystals.

From the perspective of materials design, "I" can be replaced by Br or Cl, and hence the absorption bandgap of $CH_3NH_3PbI_3$, $CH_3NH_3PbBr_3$, and $CH_3NH_3PbCl_3$ are 1.6, 1.95, and 2.46 eV [20], respectively, so the absorption bandgap will increase with the decrease of halogens' atomic number. For application, it can be used with different ratios of halogen to achieve colorful commercial applications. However, the greater the absorption bandgap, the lower the amount of sunlight that can be absorbed. Also, the toxicity of heavy metal Pb is a key factor hindering the development of perovskite solar cells; thus, one of the directions for future

development is to use nontoxic Sn to replace Pb. As the conduction band of $CH_3NH_3SnI_3$ is 0.24 eV lower than that of $CH_3NH_3PbI_3$, $CH_3NH_3SnI_3$ has a lower absorption bandgap at about 1.3 eV [21]. So far, the maximum PCE of $CH_3NH_3SnI_3$-based photovoltaics is about 5.2%, so there is still a lot of room for improvement in the material and device production.

For the part of the organic molecules, based on the theoretical calculation, Walsh proposed in October 2013, that the absorption bandgap of NH_4PbI_3 could decrease to 1.20 eV by replacing CH_3NH_3 with NH_4, which was expected to absorb more sunlight [17]. That following year, Walsh pointed out that the carrier recombination rate [22] in the perovskite absorbers was strongly associated with the strength of electric dipole moment of the organic cation, and he suggested that the use of larger electric dipole moments of CF_3NH_3 to replace CH_3NH_3 could decrease the carrier recombination rate in the perovskite absorbers. In January 2014, Snaith used $HC(NH_2)_2$ to replace CH_3NH_3 and formed $HC(NH_2)_2PbI_3$ to obtain a lower absorption bandgap at about 1.48 eV, and the PCE of $HC(NH_2)_2PbI_3$-based photovoltaics reached 14.2% [23]. In August 2014, Park produced $HC(NH_2)_2PbI_3$ on the substrate of mesoporous TiO_2/FTO and obtained device PCE of up to 16% [24]. Although the exciton diffusion length in perovskite materials could reach to micrometers, the thickness of light absorption materials in perovskite-based photovoltaics shall be controlled at around 300 to 400 nm to obtain a better PCE: the optimal short-circuit current density (J_{SC}) is about 22 mA/cm^2, depending on the thickness and bandgap of light absorption materials; the maximum open circuit voltage (V_{OC}) is about 1.1 V depending on device structure; and the optimal fill factor (FF) is about 75%, which is lower than the FF of gallium arsenide photovoltaics (FF = 86%) [25]. Recently, a high PCE of 20.2% was achieved using $HC(NH_2)_2PbI_3$ ($FAPbI_3$) as the light absorber in photovoltaics [26].

The FF of photovoltaics indicates the recombination status—the carriers will recombine inside and on the interface of light absorption materials. When the light absorption materials are thicker, the carrier recombination mainly occurs inside the light absorption materials. The decrease of thickness of the light absorption material will reduce the amount of absorbed sunlight, resulting in a decrease in short-circuit current density. For the same light absorption material, the appropriate thickness can be calculated by the product of optimal J_{sc} and FF. At present, there are theoretical calculations for optimizing the thickness of perovskite light absorption materials [27], but there are still no experimental results on the relationship between the changes in thickness of perovskite absorbers and the PCE of photovoltaics.

3. Exciton and carrier in perovskite materials

The energy is obtained by absorbing the photon, and thus the electron is excited from the ground state shifting to the excited state. Such an excited state can be regarded as an electron and a hole that is bound together by electrostatic attraction, and such an electron–hole pair is called an exciton.

Figure 2 shows when the electron in the ground state is excited to the excited state in perovskite materials, such an electron in the excited state will be called a hot electron. The hot electron can interact with the crystal lattice to generate coherent and incoherent collisions with two

different paths back to the ground state and the conduction band. Raman scattering signal is generated by the coherent collision caused by hot electrons and lattice vibration. However, as the frequency of the hot electron vibration is much higher than that of the lattice vibration, Raman scattering signal strength is very weak. On the other hand, after the incoherent collision produced by the interaction between hot electrons and lattice vibration, the electron which is relaxed in the conduction band is called a cold electron. At this time, the electrons in the conduction band and the holes in the valence band will form excitons. For CH$_3$NH$_3$PbI$_3$ absorbers, the lifetime of hot electrons is about 1 ps [28], and the exciton lifetime associated with the material structure is approximately 10–100 ns.
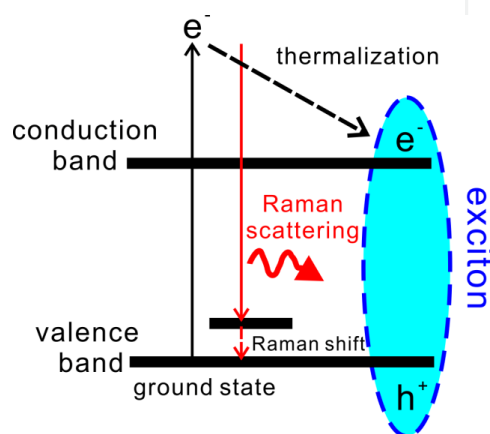

Figure 2. Energy relaxation pathways of photoexcited electrons.

Exciton binding energy is a very important parameter for the light absorption materials of photovoltaics. When the exciton in the heterogeneous interface of different materials is dissociated by the built-in electric field and becomes a free electron and hole after overcoming the binding energy. The exciton binding energy for organic materials is about 150 to 1000 meV, so with the exciton dissociation at the region of charge transfer radius, the potential difference of p–n interface must be larger than the exciton binding energy. Taking P3HT/PCBM as an example, the exciton binding energy of P3HT is about 300 meV, and LUMO potential difference of P3HT-PCBM interface is about 800 meV (3.9–3.1 eV); therefore, the exciton in the P3HT-PCBM interface can be smoothly dissociated with approximately 1.2 ps exciton dissociation time [29]. The exciton binding energy of CH$_3$NH$_3$PbI$_3$ is smaller than 50 meV but higher than the thermal energy of room temperature (K$_{BT}$ = 25.6 meV, T = 25°C). Therefore, about half of the excitons will self-dissociate to become free carriers at room temperature [30], and the other half of the excitons will have to diffuse to the interface to dissociate and become free carriers (electrons and holes).

The electrons and holes formed by the self-dissociation of excitons at room temperature must not recombine, and each has to transport to the electrodes to form a photocurrent. In March 2014, Walsh, based on theoretical calculations, predicted that the transporting paths of electrons and holes inside CH$_3$NH$_3$PbI$_3$ are different (see Figure 3) [22], and estimated that the carrier recombination rate in CH$_3$NH$_3$PbI$_3$ was very low. The arrow direction shown in Figure

3 is the orientation of the CH_3NH_3 cation (electric dipole). Electrons move along the lowest potential (blue arrow) while the holes flow along the maximum potential (red arrow). Therefore, the electric dipole of the organic cation would affect the recombination probability of electrons and holes. Also Walsh pointed out that the CF_3NH_3 cations with larger electric dipole moments should be able to effectively reduce the carrier recombination rate in perovskite absorbers.
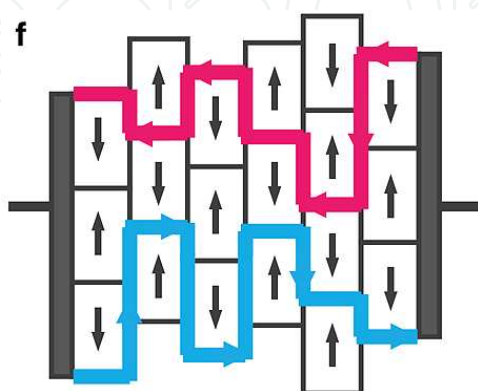

Figure 3. The propagation pathways of electrons and holes in $CH_3NH_3PbI_3$ [22].

4. Device architecture and manufacturing process of perovskite-based photovoltaics

Perovskite-based photovoltaics with more than 17% PCE can be grouped into three structures: the dye-sensitized solar cell structures, regular-type organic photovoltaic structures, and inverted-type organic photovoltaic structures. The dye-sensitized solar cell structures, based on the process order, includes FTO-conductive glass substrate/TiO_2 compact layer/mesoporous TiO_2/$HC(NH_2)_2PbI_3$ perovskite absorber/PTAA hole transporting layer/Au and its currently published maximum PCE is 20.2% [26]. For regular-type organic photovoltaic structures, its process sequence is ITO-conductive glass/PEDOT:PSS/$CH_3NH_3PbI_3$ perovskite absorber/PCBM electron transport layer/Al and its currently published maximum PCE is 17.8% [29]. For inverted-type organic photovoltaic structures, its process sequence is ITO-conductive glass/PEIE/Y:TiO_2/$CH_3NH_3PbI_{3-x}Cl_x$ perovskite absorber/Spiro-OMeTAD hole transport layer/Au, and its currently published maximum PCE is 19.3% [12]. Currently, the manufacturing process of a regular-type organic photovoltaic structure is the easiest.

Much research has been conducted on the energy conversion of perovskite-based photovoltaics in the last two years, mainly because perovskite absorbers can be produced through simple solution process methods. The main fabrication methods include one-step and two-step solution processes. The one-step method is first adopted so that the precursor of perovskite materials is dissolved in dimethyl formamide (DMF), followed by soaking of the perovskite materials on the substrate. However, the biggest drawback of this method is the

poor coating for the film, which can easily result in short-circuits due to the contact between the upper and lower electrodes. The use of an appropriate upper electrode can reduce the incidence of short-circuits [32]. As shown in Figure 4, using p-type P3HT can fill the pores of $CH_3NH_3PbI_{3-x}Cl_x$ thin films. The addition of a small amount of 1,8-diiodooctane (DIO) inside the perovskite precursors [33] can effectively reduce the generation of voids. In addition, the perovskite film with high coverage can also be obtained on the rough FTO substrate. Thus, the surface properties of the substrate have an essential effect on the continuity of perovskite thin film.
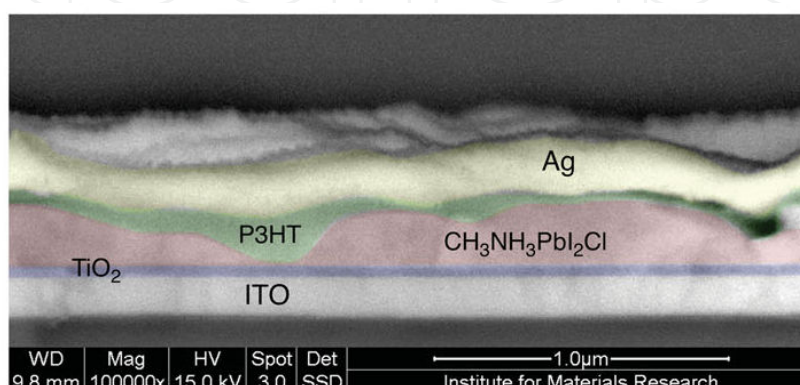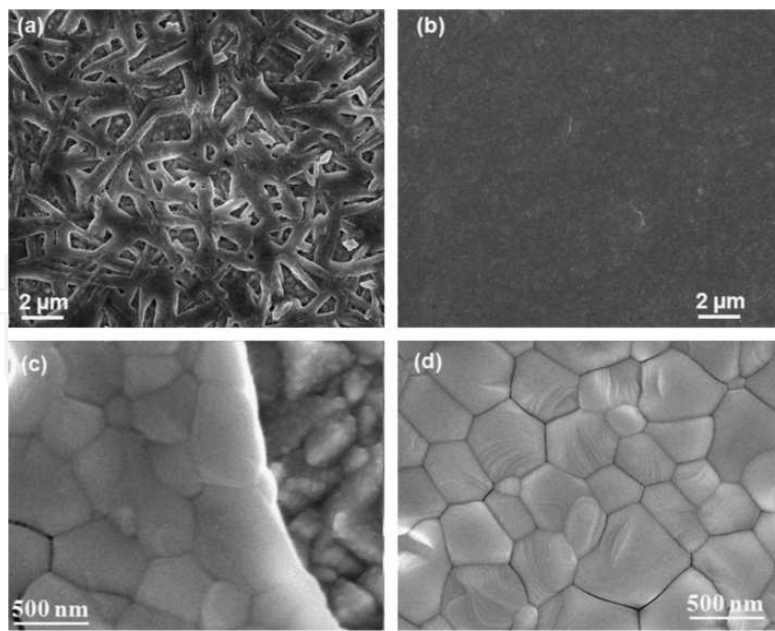

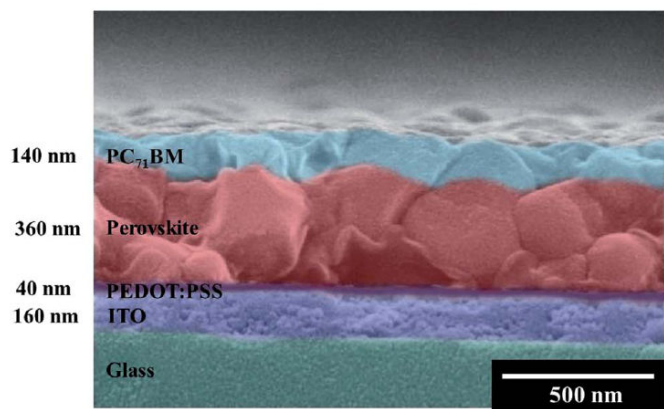**Figure 4.** Cross-sectional view of device under a scanning electron microscope [30].

In July 2014, Spiccia and Seok spontaneously used organic solvent (chlorobenzene or toluene) [34,35] to inject perovskite precursor thin films during the spin coating process, which can greatly enhance the film continuity of perovskite thin films. In September 2014, Cheng sprayed argon gas positively into the substrate to improve the solvent evaporation speed in the spin coating process of perovskite precursors and achieved up to 16.97% PCE. Figure 5 shows that perovskite thin films with argon gas processing have good film continuity and crystallinity; on the contrary, the surface of perovskite thin films without gas treatment would appear as reticular defect structures [36]. In November 2014, Jen used different solvents (toluene, chlorobenzene, and dichlorobenzene) to fabricate perovskite thin films with high continuity on top of PEDOT:PSS/ITO/glass substrate, and obtained a high PCE of 13.7% [37]. Moreover, in the manufacturing process, when the heating temperature decreases from 100°C down to 70°C, the photovoltaics still have excellent PCE of 12%. Therefore, such low-temperature deposition manufacturing techniques can be integrally applied to soft substrates.

Bruschka and Pellet from EPFL were the first to adopt a two-step coating method [9] to produce perovskite materials in the porous TiO_2 substrates. They first used a spin coating process for even distribution of PbI_2 on the mesoporous TiO_2 thin films, and then soaked the substrate into the IPA solvent with solved CH_3NH_3I. Hence, the PbI_2 on the TiO_2 surface would be reacted to $CH_3NH_3PbI_3$. Using a long-term interdiffusion process [38], the two-step solution process method can also produce high continuity of perovskite thin films on a flat PEDOT:PSS/ITO/glass substrate, which is shown in Figure 6.
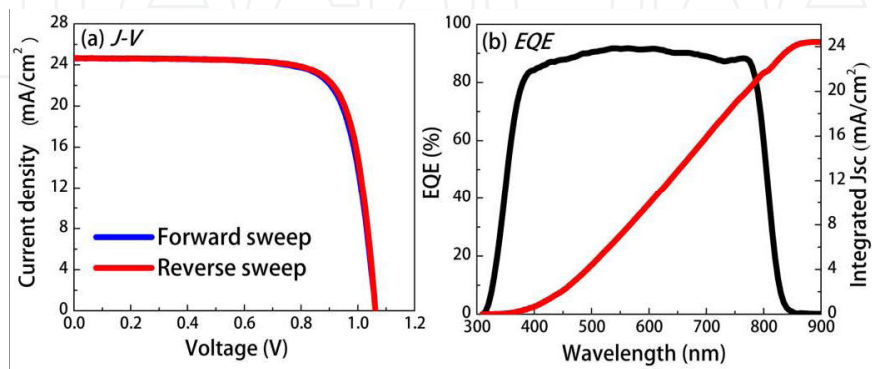
Figure 5. Scanning electron microscopy image of the $CH_3NH_3PbI_3$ surface: (a) and (c) are fabricated without argon gas; (b) and (d) are fabricated with argon gas [36].

Figure 6. Cross-sectional view of multilayer film under a scanning electron microscope [11].


Figure 7. The J–V curves and external quantum efficiency (EQE) spectrum of $CF_3NH_3PbI_3$–based photovoltaics [26].

At present, among the perovskite thin film production methods with three matching photovoltaic structures and two fabrication methods, the two-step solution process method can obtain the highest PCE of 20.2% but has the longest manufacturing process, and its photovoltaic performances are shown in Figure 7. In addition, the one-step solution process method with argon gas treatment, although with a slightly lower PCE of 16.97%, can save the most time and is suitable for making large area high-quality perovskite thin films.

5. Exciton properties in the interface between metal particles and perovskite absorbers

In order to be able to simultaneously improve the J_{SC} and FF of perovskite-based photovoltaics, we calculate the exciton properties generated by the nanoplasmonic structure embedded in perovskite absorbers to analyze the effects of nanoplasmonic structures on the properties of perovskite-based photovoltaics.

The essential parameters for electromagnetic simulations are optical parameters (refractive index and absorption coefficient), using a transfer-matrix method with Lorentz model to describe the dielectric constant of the perovskite absorber. Figure 8 shows the transmittance spectrum of perovskite/substrate, which are used for calculating the refractive index and extinction coefficient of perovskite absorber, as shown in Figure 9. Moreover, we buried a nanoplasmonic structure inside the perovskite thin film (see Figure 10), and selected appropriate structure parameters (the period = 100 nm and the metal ellipsoid length = 150 nm). Figure 11 shows the absorption spectra of nanoplasmonic structures embedded in perovskite absorber with different ellipsoid gap. When the distance between the ellipsoid is 30 nm (the short axis of the ellipsoid is 70 nm), it has a better absorption enhancement effect; at the same time, when the thickness of the perovskite absorber is decreased to 300 nm, it is expected to have a better FF.
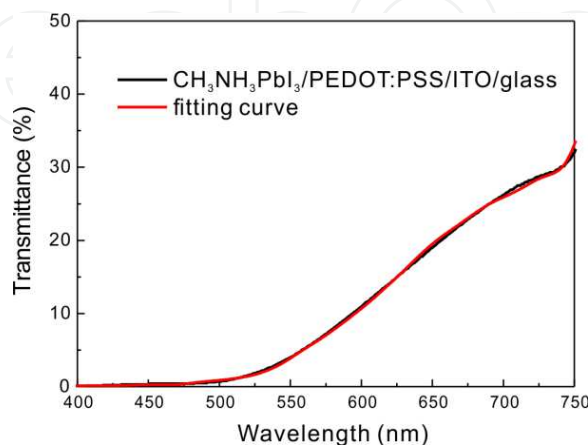
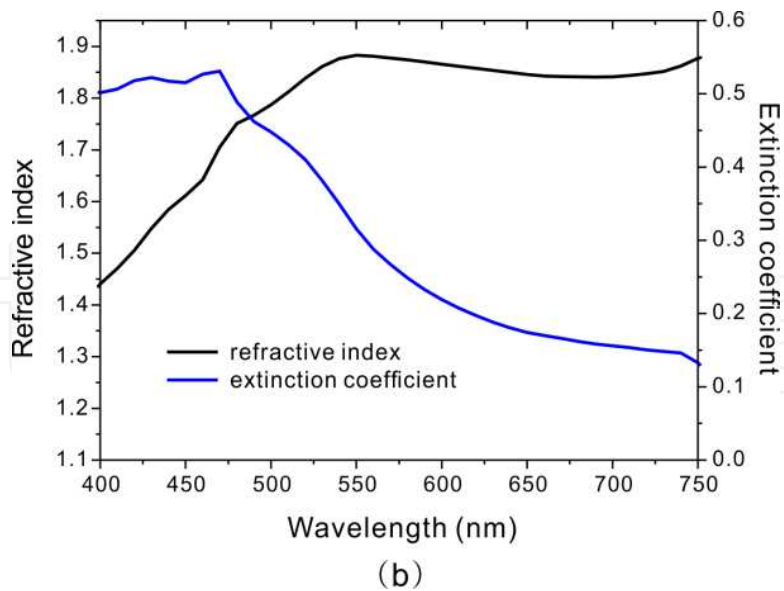

Figure 8. Transmittance spectra of CH₃NH₃PbI₃/substrate [39].

Figure 9. Refractive index and extinction coefficient of $CH_3NH_3PbI_3$ thin film [39].
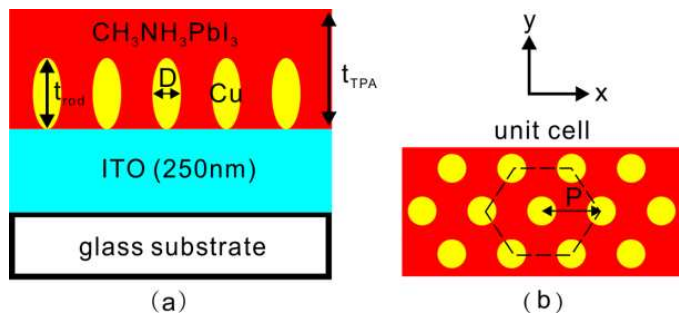

Figure 10. Side view and top view of nanoplasmonic structure embedded in the perovskite absorber [39].
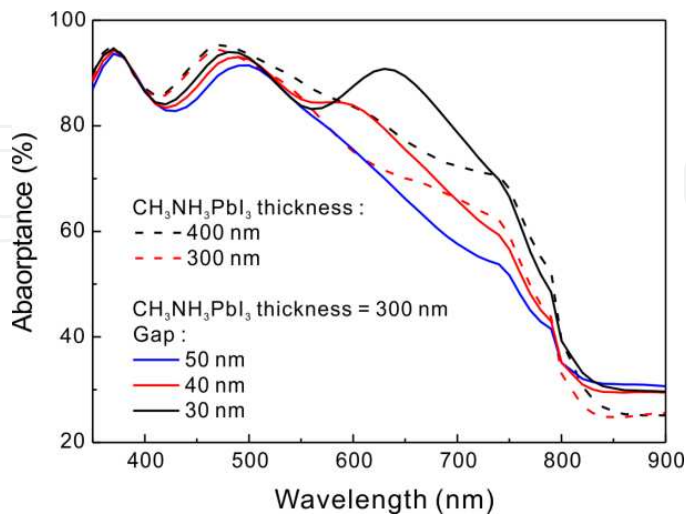

Figure 11. Absorption spectra of nanoplasmonic structures embedded in perovskite absorber with different structure parameters [39].

The nanoplasmonic structures enhanced absorptions have currently been realized in the organic solar cells [40]. However, the effect of the spatial distribution of the exciton around nanoplasmonic structures is seldom discussed. Figure 12 shows the spatial distribution of electric field (exciton). When the sunlight transmits from the ITO/glass substrate to the nanoplasmonic structure, the light field is localized at the interface between the $CH_3NH_3PbI_3$ and the Cu ellipsoid, thus most of the excitons are generated at the interface, and the exciton can be dissociated at the interface between $CH_3NH_3PbI_3$ (valance band = –5.4 eV) and Cu (Fermi energy level = –4.94 eV). After the exciton dissociation, the hole can propagate along the Cu ellipsoid to the ITO electrode, while the electron can propagate along the $CH_3NH_3PbI_3$, which will help to inhibit the carrier recombination inside the $CH_3NH_3PbI_3$. Thus, the introduction of the nanoplasmonic structure can improve the FF of $CH_3NH_3PbI_3$-based photovoltaics while enhancing the light absorption.
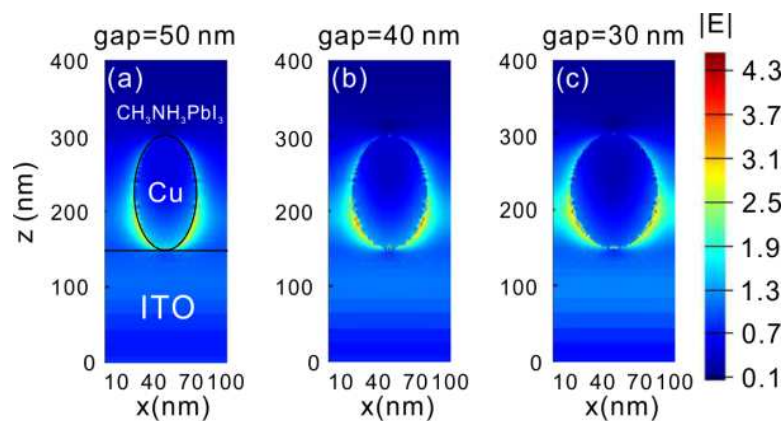
Figure 12. The distribution of the electric field (exciton) with different ellipsoid gap [39].

6. Future development direction

The PCE of GaAs single-junction photovoltaics is 28.9%, which is the closest to the Shockley–Queisser (SQ) limit of 33.7%. According to SQ theory, if the photon energy is larger than the energy gap (E_g) of light absorption materials, the energy of the incident photon will be converted from the electron to the excited state. The electron in the excited state (hot electron) and lattice will have incoherent collision and then relax to the conduction band to form exciton with the hole in the valence band, and such excitons must be dissociated to generate photocurrent. Also, assuming that the remaining energy of the absorbed photon (E_P = 2.26 eV) after thermal relaxation is equal to the energy gap of the material (E_g = 1.43 eV), so if a photon can produce a free electron, the voltage loss of this photoelectric conversion process is 0.83 V (E_P/e-E_g/e). Additionally, we can also use a simple formula to evaluate the SQ limit:

$$PCE = A \times FF \times (E_g / E_P),$$

(1)

where *PCE* is theoretical PCE, *A* is the amount of sunlight which can be absorbed by the material, and *FF* is fill factor. Taking GaAs and $CH_3NH_3PbI_3$ as examples, their SQ limits are 32.7% (0.6 × 0.86 × 1.43/2.26) and 26.6% (0.5 × 0.75 × 1.6/2.26), respectively, which indicates that the solar cells with $CH_3NH_3PbI_3$ as the main material still have space to improve.

In the past ten years, low production costs have been an advantage for organic photovoltaics and dye-sensitized solar cells, but the PCE is always less than 15%. Except that the absorption bandgap of materials cannot be effectively extended to the near-infrared region, the interaction between the light and the material is also the reason for the constrained efficiency. Taking P3HT-based photovoltaics for example, they are constrained by the exciton binding energy (~300 meV) and exciton diffusion length (~10 nm), and they must use the p–n interface with larger potential difference ($\triangle V_{P3HT-ICBA} = 0.64$ V) and blended thin film structure (P3HT:ICBA) in order to effectively convert excitons into the photocurrent. If we use formula (1) to estimate the theoretical PCE of P3HT:ICBA, E_g has to be replaced with eV_{OC} to obtain a PCE of 8.16% (0.32 × 0.75 × 0.87/2.26), which is much closer to the experimental value (7.4%) [41]. In addition, the absorption bandgap and the exciton binding energy seem to limit the development of organic photovoltaics. Table 2 indicates different photovoltaic performances and the characteristics of light absorption materials, and exciton binding energy of organic P3HT is much larger than inorganic materials (E_b < 20 meV). Also noteworthy is the Raman shift of organic materials (1000 to 1700 cm^{-1}), which is larger than that of inorganic materials (<600 cm^{-1}), even much larger than Raman scattering of $CH_3NH_3PbI_3$ (Pb-I stretching: 91 cm^{-1}). Also, the phonon energy of organic materials is much larger than that of inorganic materials. Because a large part of the energy is converted into thermal energy after the photons are absorbed by organic materials, it thus restricts the development of organic photovoltaics and dye-sensitized solar cells.

| Absorber	V_{OC} (V)	PCE (%)	E_g (eV)	E_b (meV)	Raman shift (cm^{-1})
GaAs	1.12	28.9	1.43	4	LO 295
Si	0.71	25.0	1.11	18	520
InP	0.88	22.1	1.34	5	LO 348
CIGS	0.72	19.8	1.2	12	Cu-S 472
CdTe	0.86	19.6	1.5	10.6	LO 162
$CH_3NH_3PbI_3$	1.13	19.3	1.6	50	LO 91
Prophyrin dye	0.91	12.3	1.79	330	1000–1700
P3HT	0.75	7.4	1.9	300	1000–1700

Table 2. Different photovoltaic performances and the characteristics of light absorption materials

According to an estimation of the SQ limit, there is still space for the development of perovskite-based photovoltaics. From the perspective of the manufacturing process, most of the research over the past two years has focused on how to enhance the continuity of the

$CH_3NH_3PbI_3$ film to avoid contact between the upper and lower electrodes, which can result in a short-circuit situation. At first, using perovskite materials with a mixture of Cl can obtain better film continuity. As the mixed amount of Cl is very small, the contribution of Cl is to decrease the crystallinity of $CH_3NH_3PbI_3$ and reduce the agglomeration of particles due to the rapid crystallization to further enhance the continuity of the films [42]. Moreover, the different surface roughness of substrate (ITO and FTO) can influence the continuously of $CH_3NH_3PbI_3$ films, $CH_3NH_3PbI_3$ fabricated in a more rough substrate will have a better film continuity, which is interpreted as a rough surface that is unfavorable for $CH_3NH_3PbI_3$ crystallization. Furthermore, organic solvent or inert gas is injected into $CH_3NH_3PbI_3$ precursors during the spin coating process, which can obtain $CH_3NH_3PbI_3$ thin films with good continuity and excellent PCE of 17.8%. In order to verify the mechanism of this method, we used a SEM, a 2D-XRD and fluorescence spectroscope to analyze $CH_3NH_3PbI_3$ thin films fabricated with and without toluene washing treatment [14].

Figure 13 shows the morphologies of $CH_3NH_3PbI_3$ thin films fabricated with and without toluene treatment. The $CH_3NH_3PbI_3$ thin film without toluene treatment appeared as a flower-like structure on rough surfaces, indicating that $CH_3NH_3PbI_3$ may have specific crystallization orientation. Additionally, the $CH_3NH_3PbI_3$ thin film with toluene treatment appeared to be a more even and continuous film.
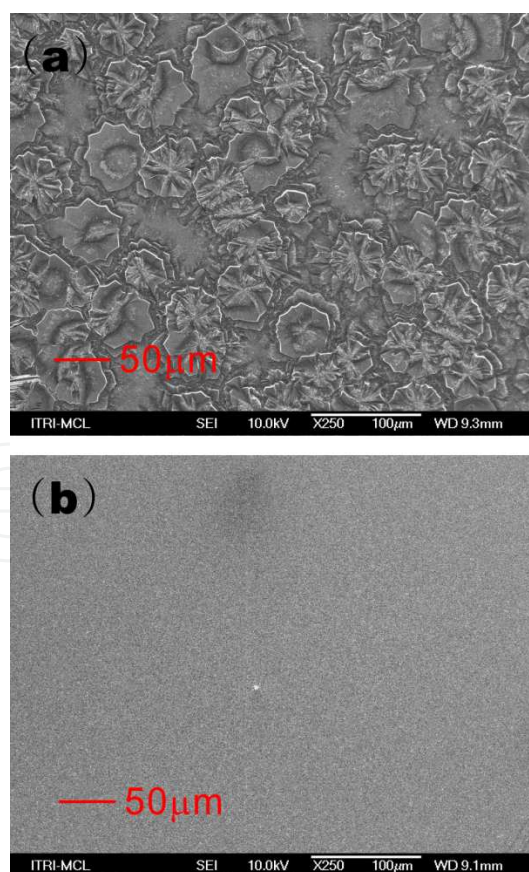
Figure 13. The SEM images of $CH_3NH_3PbI_3$ thin films; (a) without toluene treatment; (b) with toluene treatment [14].

In order to understand the crystallization orientation of $CH_3NH_3PbI_3$ materials, we use 2D-XRD as a detection tool. Figure 14 shows 2D-XRD images with and without toluene treatment. For the $CH_3NH_3PbI_3$ thin film without toluene treatment, the preferred orientation of the crystallization tendency is at (112), while the $CH_3NH_3PbI_3$ thin film with toluene treatment has no specific crystallization orientation, which indicates that $CH_3NH_3PbI_3$ precursors with the toluene treatment will interfere with the crystallization of $CH_3NH_3PbI_3$ and thus obtain more smooth and continuous $CH_3NH_3PbI_3$ thin films. Analysis of the FWHM of X-ray diffraction peak can also obtain the crystal domain size of $CH_3NH_3PbI_3$ thin films with and without toluene treatment at 17.6 nm and 29.6 nm, respectively, indicating that the toluene treatment indeed inhibited the crystallization of $CH_3NH_3PbI_3$.
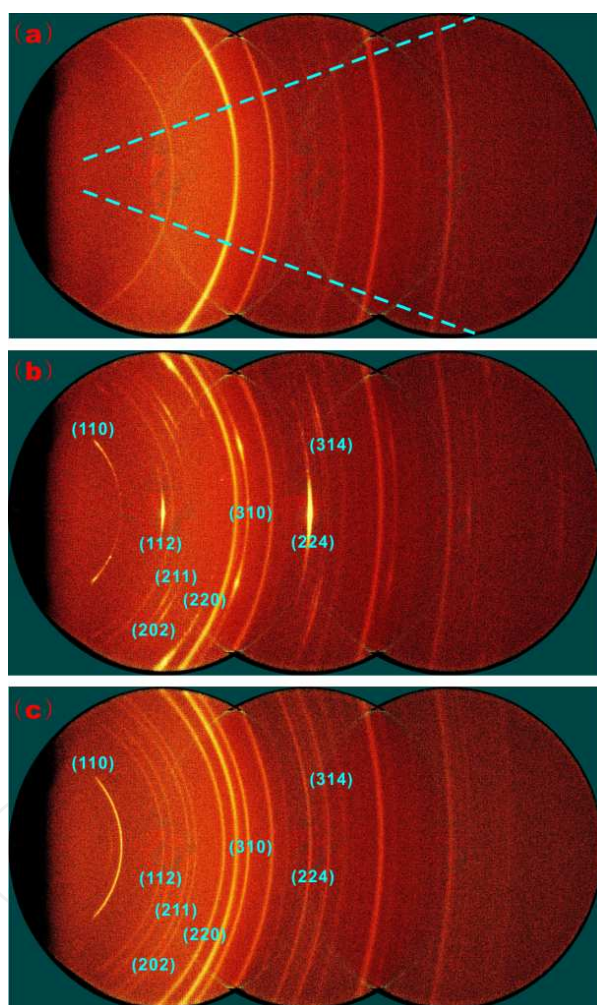
Figure 14. Two-dimensional X-ray diffraction patterns: (a) PEDOT:PSS/ITO/glass; (b) $CH_3NH_3PbI_3$/PEDOT:PSS/ITO/glass without toluene treatment; (c) $CH_3NH_3PbI_3$/PEDOT:PSS/ITO/glass with toluene treatment [14].

Figure 15 displays the absorbance spectra of perovskite absorbers on PEDOT:PSS/ITO/glass substrate fabricated with and without the toluene treatment. The perovskite films have two absorption peaks at ~480 nm and ~750 nm, which indicate the formation of $CH_3NH_3PbI_3$. When neglecting the reflectance, the absorbance can be treated as absorption. The absorp-

tion coefficient can be obtained by $\alpha = A/D$, where A is the absorbance, and D (~260 nm) is the film thickness measured by an α step. The absorption coefficient of the $CH_3NH_3PbI_3$ film fabricated with (without) the toluene treatment is 6.02×10^4 cm^{-1} (4.63×10^4 cm^{-1}) at a wavelength of 479 nm.
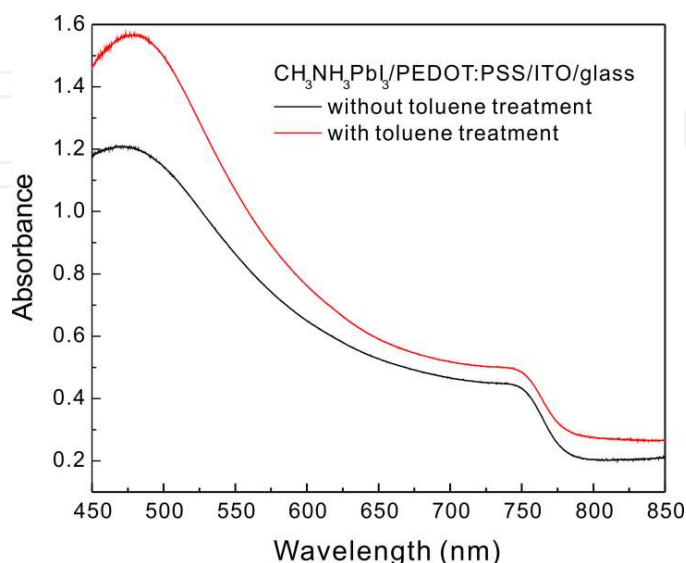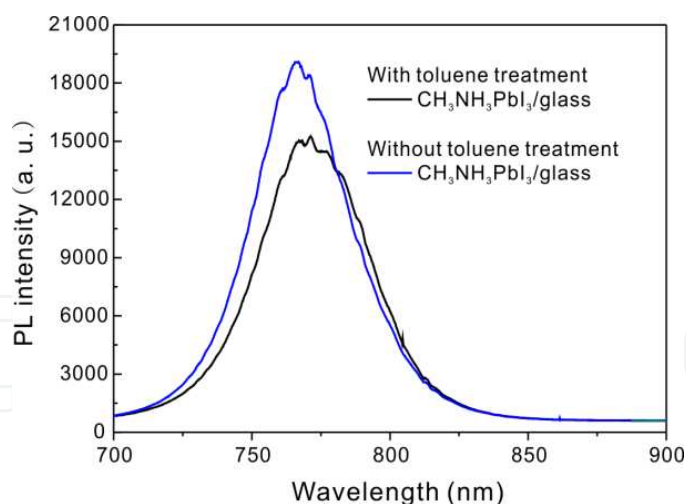

Figure 15. Absorbance spectra of $CH_3NH_3PbI_3$/PEDOT:PSS/ITO/glass without and with toluene treatment [14].

In order to understand the exciton characteristics of the CH_3NH_3PbI thin film with toluene treatment, we measured the fluorescence spectra of the sample, as shown in Figure 16. The $CH_3NH_3PbI_3$ thin film with toluene treatment had weaker fluorescence, showing that the excitons in the $CH_3NH_3PbI_3$ thin film with toluene treatment had shorter lifetimes. The experimental data showed that the toluene treatment can improve the continuity of $CH_3NH_3PbI_3$ thin films but inhibit crystallinity, leading to a reduction in the exciton's lifetime. In addition, we also used this method to fabricate photovoltaics with structures starting with the substrate sequentially to glass/ITO/PEDOT:PSS/$CH_3NH_3PbI_3$/PCBM/Ag, and the obtained highest PCE was 11.7% (V_{OC} = 0.92 V, J_{SC} = 18.2 mA/cm^2, FF = 0.7) [14], which proves that toluene-treated CH_3NH_3PbI can be used as a light absorption material for excellent PCE.

Although the $CH_3NH_3PbI_3$ absorbers with toluene treatment have good continuity, and the PCE can easily exceed 10%, the morphologies of these perovskite thin films and exciton properties showed that the substrate in the absence of specific crystallization orientation has to sacrifice the crystallinity of perovskite thin films to achieve the good continuity, which could produce high-efficiency photovoltaics through solution process methods. Therefore, we believe that it is necessary to find substrates with crystallinity or specific structure for the production of perovskite-based photovoltaics in order to manufacture perovskite absorbers with both high continuity and crystallization by solution process methods to be able to improve the V_{OC} and FF of the photovoltaics.

Since the hot electron lifetime of $CH_3NH_3PbI_3$ is about 1 ps, high conductive nanostructures can be used to improve the efficiency of hot electron injection from $CH_3NH_3PbI_3$ to electron

Figure 16. The photoluminescence spectra of $CH_3NH_3PbI_3$ thin films [14].

acceptors. The issue of hot electron injection and multiple exciton generation has been widely discussed in studies of quantum dot–sensitized solar cells. In theoretical estimation, the limit of the PCE of the photovoltaics with hot electron injection is 42% [43], which is higher than the SQ limit of 33.7%. Therefore, we predicted that if we use ZnO with nanorod structures to collect hot electron injection, it should be able to improve the V_{OC} of perovskite-based photovoltaics. Because the hot electrons inject into ZnO at a higher energy potential, and if the conductivity of ZnO remains high enough that the hot electrons are able to maintain its energy potential transporting to the electrode, then higher V_{OC} should be achieved.

Moreover, in the aging test of perovskite solar cells, Park conducted tests measuring the stability of PCE under different humidity storage conditions [44]. Under 55% relative humidity, the PCE of $CH_3NH_3PbI_3$-based photovoltaics decreased from 11% to 3.5% after 20 days of storage. In addition, if using $CH_3NH_3PbI_{2.4}Br_{0.6}$ as the light absorption material under the same storage conditions (55% relative humidity), the PCE could be maintained at 9.5% for 20 days. Although "I" of the $CH_3NH_3PbI_3$ was replaced by Br, which could improve the stability of perovskite-based photovoltaics, an increase of the Br substituted amount would also increase the absorption bandgap of the perovskite materials, which would result in the decrease of PCE from 11% to 9.5%, at the expense of light absorption. The results for aging tests of long-term exposure to sunlight have not yet been published in internationally important journals. As a result, it is still doubtful whether perovskite photovoltaics have long-term stability, which shall be further tested under actual conditions for the properties of the high PCE of perovskite-based photovoltaics.

7. Conclusion

The power conversion efficiency (PCE) of perovskite-based photovoltaics have exceeded 20%, and the efficiency in different types of substrates by solution process methods can reach over

17%, indicating that there is very high possibility for commercializing perovskite-based photovoltaics. However, the light absorption materials contain Pb, which is the biggest obstacle for commercialization of perovskite-based photovoltaics. The absorption bandgap of CH$_3$NH$_3$SnI$_3$ with Pb replaced with Sn is about 1.3 eV, which is a promising light absorption material. So far, the highest PCE of CH$_3$NH$_3$SnI$_3$-based photovoltaics is about 5.2% far away from the Shockley–Queisser limit of 33.7%. Therefore, research on CH$_3$NH$_3$SnI$_3$-based photovoltaics have been slowed due to the benefit issues, and thus it is essential to conduct more basic research to further evaluate the limits of perovskite-based photovoltaics for the arrival of earlier commercialization process.

Acknowledgements

Author details

Sheng Hsiung Chang[1*], Hsin-Ming Cheng[2], Sheng-Hui Chen[3] and Kuen-Feng Lin[1,3]

*Address all correspondence to: shchang@ncu.edu.tw

1 Research Center for New Generation Photovoltaics, National Central University, Taoyuan, Taiwan, ROC

2 Material and Chemical Research Laboratories, Industrial Technology Research Center, Hsinchu, Taiwan, ROC

3 Department of Optics and Photonics, National Central University, Taoyuan, Taiwan, ROC

References

[1] J. G. Bednorz and K. A. Muller. Perovskite-type oxides—The new approach to high-Tc superconductivity. *Reviews of Modern Physics* 60 (1988) 585–600.

[2] T. He, Q. Huang, A. P. Ramirez, Y. Wang, K. A. Regan, N. Rogado, M. A. Hayward, M. K. Haas, J. S. Slusky, K. Inumara, H. W. Zandbergen, N. P. Ong, and R. J. Cava. Superconductivity in the non-oxide perovskite MgCNi$_3$. *Nature* 411 (2001) 54–56.

[3] G. Xing, N. Mathews, S. Sun, S. S. Lim, Y. M. Lam, M. Gratzel, S. Mhaisalkar, and T. C. Sum. Long-range balanced electron- and hole-transport lengths in organic–inorganic $CH_3NH_3PbI_3$. *Science* 342 (2013) 344–347.

[4] K. Tanaka, T. Takahashi, T. Ban, T. Kondo, K. Uchida, and N. Miura. *Solid State Communications* 127 (2003) 619–623.

[5] M. Era, S. Morimoto, T. Tsutsui, and S. Saito. Organic–inorganic heterostructure electroluminescent device using a layered perovskite semiconductor (C6H5C2H4NH3)2PbI4. *Applied Physics Letters* 65 (1994) 676–678.

[6] A. Kojima, K. Teshima, Y. Shirai, and T. Miyasaka. Organometal halide perovskite as visible-light sensitizers for photovoltaic cells. *Journal of the American Chemical Society* 131 (2009) 6050–6051.

[7] L. Etgar, P. Gao, Z. Xue, Q. Peng, A. K. Chandiran, B. Liu, Md. K. Nazeeruddin, and M. Gratzel. Mesocopic $CH_3NH_3PbI_3/TiO_2$ heterojunction solar cells. *Journal of The American Chemical Society* 134 (2012) 17396–17399.

[8] Michael M. Lee, Joël Teuscher, Tsutomu Miyasaka, Takurou N. Murakami, Henry J. Snaith. Efficient hybrid solar cells based on meso-superstructured organometal halide perovskites. *Science* 338 (2014) 643–647.

[9] J. Burschka, N. Pellet, S-J. Moon, R. Humphry-Baker, P. Gao, M. K. Nazeeruddin, and M. Gratzel. Sequential deposition as a route to high-performance perovskite-sensitized solar cells. *Nature* 499 (2013) 316–319.

[10] M. Liu, M. B. Johnston, and H. J. Snaith. Efficient planar heterojunction perovskite solar cells by vapour deposition. *Nature* 501 (2013) 395–398.

[11] C-H. Chiang, Z-L. Tseng, and C-G. Wu. Planar heterojunction perovskite/PC71BM solar cells with enhanced open-circuit voltage via a (2/1)-step spin-coating process. *Journal of Materials Chemistry A* 2 (2014) 15897–15903.

[12] H. Zhou, Q. Chen, G. Li, S. Luo, T-B. Song, H-S. Duan, Z. Hong, J. You, Y. Liu, and Y. Yang. Interface engineering of highly efficient perovskite solar cells. *Science* 345 (2014) 542–546.

[13] J-H. Im, I-H. Jang, N. Pellet, M. Gratzel, and N-G. Park. Growth of $CH_3NH_3PbI_3$ cuboids with controlled sized for high-efficiency perovskite solar cells. *Nature Technology* 9 (2014) 927–932.

[14] K-F. Lin, S-H. Chang, K-H. Wang, H-M. Cheng, K. Y. Chiu, K-M. Lee, S-H. Cheng, and C-G. Wu. Unraveling the high performance of tri-iodide perovskite absorber based photovoltaics with a non-polar solvent washing treatment. *Solar Energy Materials and Solar Cells*, accepted for publication.

[15] W-J. Yin, T. Shi, and Y. Yan. Unusual defect physics in $CH_3NH_3PbI_3$ perovskite solar cell absorber. *Applied Physics Letters* 104 (2014) 063903.

[16] M. Hirasawa, T. Ishihara, T. Goto, K. Uchida, and N. Miura. Magnetoabsorption of the lowest exciton in perovskite-type compound (CH₃CH₃)PbI₃. *Physica B: Condensed Matter* 201 (1994) 427–430.

[17] F. Brivio, A. B. Walker, and A. Walsh. Structural and electronic properties of hybrid perovskites for high-efficiency thin-film photovoltaics from first-principles. *APL Materials* 1 (2013) 042111.

[18] Z. Guo, J. S. Manser, Y. Wan, P. V. Kamat, and L. Huang. Spatial and temporal imaging of long-range charge transport in perovskite thin films by ultrafast microscopy. *Nature Communications* 6 (2015) 7471.

[19] S. D. Stranks, G. E. Eperon, G. Grancini, C. Menelaou, M. J. P. Alcocer, T. Leijtens, L. M. Herz, A. Petrozza, and H. J. Snaith. Electron–hole diffusion lengths exceeding 1 micrometer in an organometal trihalide perovskite absorber. *Science* 342 (2013) 341–344.

[20] K. T. Butler, J. M. Forst, and A. Walsh. Band alignment of the hybrid halide perovskites CH₃NH₃PbCl₃, CH₃NH₃PbBr₃, and CH₃NH₃PbI₃. *Materials Horizons* accepted 28 Oct. 2014 (DOI: 10.1039/C4MH00174E).

[21] F. Hao, C. C. Stoumpos, D. H. Cao, R. P. H. Chang, and M. G. Kanatzidis. Lead-free solid-state organic–inorganic halide perovskite solar cells. *Nature Photonics* 8 (2014) 489–494.

[22] J. M. Frost, K. T. Butler, F. Brivio, C. H. Hendon, M. van Schilfgaarde, and A. Walsh. Atomistic origins of high-performance in hybrid halide perovskite solar cells. *Nano Letters* 14 (2014) 2584–2590.

[23] G. E. Eperon, S. D. Stranks, C. Menelaou, M. B. Johnston, L. M. Herz, and H. J. Snaith. Formamidinium lead trihalide: a broadly tunable perovskite for efficient planar heterojunction solar cells. 7 (2014) 982–988.

[24] J-W. Lee, D-J. Seol, A-N. Cho, and N-G. Park. High-efficiency perovskite solar cells based on the black polymorph of HC(NH₂)₂PbI₃. *Advanced Materials* 26 (2014) 4991–4998.

[25] M. A. Green, K. Emery, Y. Hishikawa, W. Warta, and E. D. Dunlop. Solar cell efficiency table (version 44). *Progress in Photovoltaics: Research and Applications* 22 (2014) 701–710.

[26] W. S. Yang, J. H. Noh, N. J. Jeon, Y. C. Kim, S. Ryu, J. Seo, and S. I. Seok. High-performance photovoltaic perovskite layers fabricated through intromolecular exchange. *Science* (DOI: 10.1126/science.aaa9272).

[27] F. Liu, J. Zhu, J. Wei, Y. Li, M. Lv, S. Yang, B. Zhang, J. Yao, and S. Dai. Numerical simulation: toward the design of high-efficiency planar perovskite solar cells. *Applied Physics Letters* 104 (2014) 25358.

[28] H-Y. Hsu, C-Y. Wang, A. Fathi, J-W. Shiu, C-C. Chung, P-S. Shen, T-F. Guo, P. Chen, Y-P. Lee, and E. W-G. Diau. Femtosecond excitonic relaxation dynamics of perovskite on mesoporous films of Al_2O_3 and NiO nanoparticles. *Angewandte Chemie* 53 (2014) 9339–9342.

[29] S. H. Chang, C-H. Chiang, H-M. Cheng, C-Y. Tai, and C-G. Wu. Broadband charge transfer dynamics in P3HT:PCBM blended film. *Optics Express* 38 (2013) 5342–5345.

[30] T. C. Sum and N. Mathews. Advancements in perovskite solar cells: photophysics behind the photovoltaics. *Energy Environmental Science* 7 (2014) 2518–2534.

[31] W. Nie, H. Tsai, R. Asadpour, J-C. Blancon, A. J. Neukirch, G. Gupta, J. J. Crochet, M. Chhowalla, S. Tretiak, M. A. Alam, H-L. Wang, and A. D. Mohite. High-efficiency solution-processed perovskite solar cells with millimeter-scale grains. *Science* 347 (2015), 522–525.

[32] B. Conings, L. Baeten, C. D. Cobbelaere, J. D'Haen, J. Manca, and H-G. Boyen. Perovskite-based hybrid solar cells exceeding 10% efficiency with high reproducibility using a thin film sandwich approach. *Advance Materials* 26 (2014) 2041–2046.

[33] P-W. Liang, C-Y. Laio, C-C. Chueh, F. Zuo, S. T. Williams, X-K. Xin, J. Lin, and A. K-Y. Jen. Additive enhanced crystallization of solution-processed perovskite for highly efficiency planar-heterojunction solar cells. *Advanced Materials* 26 (2014) 3748–3754.

[34] M. Xiao, F. Huang, W. Huang, Y. Dkhissi, Y. Zhu, J. Etheridge, A. Gray-Weale, U. Bach, Y-B. Cheng, and L. Spiccia. A fast deposition-crystallization procedure for highly efficient lead iodide perovskite thin-film solar cells. *Angewandte Chemie* 126 (2014) 10056–10061.

[35] N. J. Jeon, J. H. Noh, Y. C. Kim, W. S. Yang, S. Ryu, and S. I. Seok. Solvent engineering for high-performance inorganic–organic hybrid perovskite solar cells. *Nature Materials* 13 (2014) 897–903.

[36] F. Huang, Y. Dkhissi W. Huang, M. Xiao, I. Benesperi, S. Rubanov, Y. Zhu, X. Lin, L. Jiang, Y. Zhou, A. Gray-Weale, J. Etheridge, C. R. McNeill, R. A. Caruso, U. Bach, L. Spiccia, and Y-B. Cheng. Gas-assisted preparation of lead iodide perovskite films consisting of a monolayer of single crystalline grains for high efficiency planar solar cells. *Nano Energy* 10 (2014) 10–18.

[37] J. W. Jung, S. T. Williams, and A. K-Y. Jen. Low-temperature processed high-performance flexible perovskite solar cells via rationally optimized solvent washing treatments. *RSC Advances* 4 (2014) 62971–62977.

[38] C. Bi, Y. Shao, Y. Yuan, Z. Xiao, C. Wang, Y. Gao, and J. Huang. Understanding the formation and evolution of interdiffusion grown organolead halide perovskite thin films by thermal annealing. *Journal of Chemistry A* 2 (2014) 18508–18514.

[39] S. H. Chang, K-F. Lin, C-H. Chiang, S-H. Chen, and C-G. Wu. Plasmonic structure enhanced exciton generation at the interface between the perovskite absorber and copper nanoparticles. *Scientific World Journal* 2014 (2014) 128414.

[40] S. H. Chang. Modeling and design of Ag, Au, and Cu nanoplasmonic structures for enhancing the absorption of P3HT:PCBM-based photovoltaics. *IEEE Photonics Journal* 5 (2013) 4800509.

[41] X. Guo, C. Cui, M. Zhang, L. Huo, Y. Huang, J. Hou, and Y. Li. High efficiency polymer solar cells based on poly(3-hexylthiophene)/indene-C70 bisadduct with solvent additive. *Energy Environmental Science* 5 (2012) 7943–7949.

[42] S. T. Williams, F. Zuo, C-C. Chueh, C-Y. Liao, P-W. Liang, and A. K-Y. Jen, Role of chloride in the morphological evolution of organo-lead halide perovskite thin films. *ACS Nano* 8 (2014) 10640–10654.

[43] M. C. Beard, A. G. Midgett, M. C. Hanna, J. M. Luther, B. K. Hughes, and A. J. Nozik. Comparing multiple exciton generation in quantum dots to impact ionization in bulk semiconductors: implications for enhancement of solar energy conversion. *Nano Letters* 10 (2010) 3019–3027.

[44] N-G. Park. Perovskite solar cells: an emerging photovoltaic technology, *Materials Today* 18 (2015) 65–72.